Nanofluid flow and heat transfer in a microchannel with interfacial electrokinetic effects

Qingkai Zhao[1, a, b] Hang Xu[1, b], Longbin Tao[c]

[a]School of Shipbuilding Engineering, Harbin Engineering University, Harbin 150001, China

[b]Collaborative Innovation Center for Advanced Ship and Deep-Sea Exploration (CISSE), State Key Lab of Ocean Engineering, School of Naval Architecture, Ocean and Civil Engineering, Shanghai Jiao Tong University, Shanghai 200240, China

[c]Department of Naval Architecture, Ocean and Marine Engineering, University of Strathclyde, Glasgow G4 0LZ, United Kingdom

Abstract *The behaviour of microchannel flow of a nanofluid between two parallel flat plates in the presence of the electrical double layer (EDL) is investigated in this paper. The problem is formulated based on the Buongiorno nanofluid model with the electrical body force due to the EDL being considered in the momentum equation. As one of the highlights of the present investigation, the unphysical assumption introduced in previous studies often leading to the discontinuities of flow field that the electrostatic potential in the middle of the channel has to be equal to zero is eliminated. In addition, the inappropriate assumption that the pressure constant is treated as a known condition is also rectified. The new model is developed with the governing equations being reduced by a set of dimensionless quantities to a set of coupled ordinary differential equations. Based on the analytical approximations, the influences of various physical parameters on the flow field and temperature field, and the important physical quantities of practical interests are analysed and discussed in detail.*

[1] These authors contributed equally.

Email:qkzhao86@163.com (Q.K. Zhao), hangxu@sjtu.edu.cn (H. Xu)

The corresponding author: longbin.tao@strath.ac.uk (L. Tao)

Keywords electrical double layer, microchannel, nanofluid, zeta potential, analytical solution

Nomenclature

A_1, A_2	constants
A_c	cross-sectional area of the microchannel [m]
c	specific heat at constant pressure[J $kg^{-1}K^{-1}$]
C	nanoparticle volume fraction [kg m^{-3}]
C_0	nanoparticle volume fraction at the microchannel entrance [kg m^{-3}]
C_w	nanoparticle volume fraction on the microchannel wall surface [kg m^{-3}] local
C_{f2}	skin friction coefficients on the lower wall of the microchannel [kg m^{-3}]
D_B	Brownian diffusion coefficient [m^2s^{-1}]
D_T	thermophoretic diffusion coefficient [m^2s^{-1}]
e	charge of a proton [C]
Ec	Eckert number
E_s	streaming potential[V]
$\bar{E}_s$	non-dimensional streaming potential
E_x	electric field strength[V m^{-1} or N C^{-1}]
$\mathbf{F}$	electrical body force [N m^{-3}]
G_1	non-dimensional parameter, represents the ratio of the mechanical force to viscous force
G_2	non-dimensional parameter, represents the ratio of EDL force to viscous force
G_3	non-dimensional parameter, represents the ratio of streaming current to conduction current
H	half distance between the upper and lower microchannel walls [m] conduction
I_c, I_s	and streaming currents, respectively [A]

k	Debye-H¨uckel parameter [m^{-1}]
k_b	Boltzmann constant [J $mol^{-1}K^{-1}$]
k_f	thermal conductivity of the fluid [W $m^{-1}K^{-1}$]
L	length of the microchannel [m]
Le	Lewis number
n_i	ionic number concentration of the ith species
n_{0i}	the bulk ionic concentration of type i ions [m^{-3}]
Nb	Brownian motion parameter
Nt	thermophoresis parameter
Nu_2	local Nusselt number on the lower wall of the microchannel
p	pressure [Pa]
Pr	Prandtl number
q_{wT2}	wall heat flux on the lower wall of the microchannel [W m^{-2}]
q_{wC2}	local wall flux of nanoparticles on the lower wall of the microchannel [kg $m^{-2}s^{-1}$]
Re	Reynolds number
Sh_2	local Sherwood number on the lower wall of the microchannel
T	temperature [K]
T_0	temperature at the microchannel entrance [K]
T_w	temperature on the microchannel wall surface [K]
$\hat{T}$	absolute temperature [K]
u	velocity of the fluid [m s^{-1}]
U	non-dimensional velocity of the fluid
U_m	average velocity of the fluid [m s^{-1}]
x, y, z	Cartesian coordinates [m]
X, Y	non-dimensional Cartesian coordinates

$\hat{z}_i$	the valence of type i ions

Greek symbols

α	thermal diffusivity of the nanofluid $[m^2 s^{-1}]$
ε	dielectric constant of the medium
ε_0	permittivity of vacuum $[\mathrm{C}\, V^{-1} m^{-1}]$
κ	non-dimensional electrokinetic separation distance between the upper and lower wall of the microchannel
λ_0	electrical conductivity of the fluid $[\Omega^{-1} m^{-1}]$
μ	dynamic viscosity of the fluid $[\mathrm{kg}\, m^{-1} s^{-1}]$
ν	kinematic viscosity of the fluid $[m^2 s^{-1}]$
Θ	non-dimensional temperature distribution
Φ	non-dimensional nanoparticle volume fraction
ρ_e	charge density $[\mathrm{C}\, m^{-3}]$
ρ_f	density of the fluid $[\mathrm{kg}\, m^{-3}]$
τ	ratio of the heat capacity of the nanoparticle to that of the fluid shear
τ_{w2}	stress on the lower wall of the microchannel [Pa]
ζ	zeta potential [V]
ψ	electrostatic potential [V]
Ψ	non-dimensional electrostatic potential

1 Introduction

The research of fluid flow and heat transfer in microchannel is of significant interest to engineers and scientists in industrial applications such as microchannel heat sinks for cooling high power very large scale integration circuitry and laser diode arrays, heat transfer

augmentation in aerospace technology, micro-reactors for the analysis of biological cells and micro fluid pumps [1,2]. However, conventional transport theories are insufficient to explain many phenomena associated with microscale flow. Experimental observations [3–5] have shown that flow and heat transfer behaviours in microscale are quite different from those in macroscale. Particularly, Wang and Peng [5] noticed that transition and laminar heat transfer in microchannels are highly strange and complicated compared with the conventionally sized situation. They conjectured that this unusual behavior of microchannel flow may be largely due to electrical double layer (EDL) effects. If the liquid contains very small number of ions, the electrostatic charges on the solid surface will attract the counterions in the liquid to establish an electrical field. The rearrangement of the electrostatic charges on the solid surface and the balancing charges in the liquid is called the EDL [6]. When a liquid is forced through a microchannel under hydrostatic pressure, the ions in the diffuse layer of the EDL are carried towards the downstream end. This causes an electrical current, called streaming current. The accumulation of ions downstream sets up an electrical field with an electrical potential called the streaming potential. This field causes a current, called conduction current, to flow back in the opposite direction. When conduction current is equal to the streaming current a steady state is reached. It is easy to understand that, when the ions are moved in the diffuse double layer, they pull the liquid along with them. However, the motion of the ions in the diffuse double layer is subject to the electrical potential of the double layer. Thus the liquid flow and associated heat transfer are affected by the presence of the EDL.

Generally, for macrochannel flow the EDL effects can be neglected since the EDL thickness is very small as compared to the channels' characteristic length. While for microchannel flow, the thickness of the EDL is comparable to the characteristic length of channels and its effect has to be considered. It is noted that the EDL effects originated from the interfacial

electrokinetic effects [7] by the variation of electric potential near a surface and could have a significant influence on the behaviour of fluid flow. Therefore, it is necessary to investigate the fundamental characteristics of these phenomena in order to develop the high quality products. Recently, Mala *et al.* [8] analyzed the effects of the EDL at the solid-liquid interface on liquid flow and heat transfer through a microchannel between two parallel plates. Mala *et al.* [9] reported experimental results on flow of distilled water and aqueous solutions through silicon and glass microchannels between two parallel plates. Ren *et al.* [10] further investigated the electro-viscous effect caused by the EDL near a solid-liquid interface in microchannels. Zhang *et al.* [11] experimentally studied the streaming potentials across a porous membrane in various organic-aqueous solutions.

On the other hand, increasing research effort has been devoted to study the mechanism of nanofluids owing to their great potentials in thermal engineering [12–14]. Many experiments were carried out to investigate convective flow and heat transfer features of various nanofluids [15–17]. Among those studies, Wen and Ding [15] experimentally confirmed that the heat transfer enhancement is prominent when pure heat transfer fluids are replaced by nanofluids. Similar conclusions were drawn by other researchers [18, 19]. Theoretically, several mathematical models such as the homogenous flow model [20], the dispersion model [21], the Buongiorno's model [22] have been suggested to predict nanofluids' behaviours. Among these models, the Buongiorno's model received great attention [23] since it explains well the slip mechanisms between the nanoparticles and the base fluid. Since the volumetric distributions of nanoparticles can be altered by virous physical processing, such as fluid flow, heat transfer, electric field, it is very attractive to investigate such multiple physical phenomena with consideration of how these physical processing interacts each other. For example, the EDL modifies the fluid motion obviously, which could affect heat transfer, and also play an important role in the volumetric distribution of the nanoparticles. Therefore,

it is necessary to investigate the influence of EDL on liquid flow of nanofluids.

This paper is to examine a steady-state, fully-developed, laminar nanofluid flow in a horizontal microchannel with the interfacial electrokinetic effects. The electrical body force resulting from the electrical double layer (EDL) and the electrokinetic fields are considered in the momentum equation. The energy and the volumetric concentration of the nanoparticles equations are established based on the Buongiorno's model. One nonphysical assumption by Mala *et al.* [8, 9] that the electrostatic potential in the middle of the channel has to be equal to zero is corrected since it can lead to the discontinuities of the flow field. The other inappropriate assumption by Mala *et al.* [8,9] and Ren *et al.* [10] that the pressure constant is a known condition is also rectified, which ensure our model to agree with commonly-accepted models in the field of fluid mechanics. The governing equation is reduced by non-dimensional variables to a set of coupled nonlinear ordinary equations. Particularly, an analytical solution for the electrical field is presented. Analytical approximations for other fields are obtained by the homotopy analysis method. The influences of various physical parameters on important physical quantities of practical interests are analysed and discussed. The studies of these fundamental phenomena and their mechanisms are helpful for the optimal design, improved performances and broad applications of micro/nanofluidic systems.

2 Analytical solution to the electrostatic potential

According to the theory of electrostatics, the relation between ψ and ρ_e is given by the Poisson's equation near a flat surface as [6, 24]

$$\frac{d^2\psi}{dy^2} = -\frac{\rho_e}{\varepsilon_0 \varepsilon}, \tag{1}$$

where ε is the dielectric constant of the fluid and ε_0 is the permittivity of vacuum.

Using the assumption of the equilibrium Boltzmann distribution about uniform dielectric constant and neglecting fluctuation, the number of ion distribution in a symmetric electrolyte solution takes the form

$$n_i = n_{0i} \exp\left(- \frac{\hat{z}_i e \psi}{k_b \hat{T}} \right), \tag{2}$$

where n_{0i} and $\hat{z}_i$ denote the bulk ionic concentration and the valence of type i ions, respectively, e the charge of a proton, ψ the electrical potential, k_b the Boltzmann's constant and $\hat{T}$ the absolute temperature. The net charge density in a unit volume of the fluid is given by

$$\rho_e = (n_+ - n_-)\hat{z}e = -2n_0 \hat{z}e \sinh\left(\frac{\hat{z}e\psi}{k_b \hat{T}} \right) \tag{3}$$

Substituting Eq.(3) into the Poisson equation (1), we obtain the well-known Poisson-Boltzmann equation

$$\frac{d^2\psi}{dy^2} = \frac{2n_0 \hat{z}e}{\varepsilon_0 \varepsilon} \sinh\left(\frac{\hat{z}e\psi}{k_b \hat{T}} \right). \tag{4}$$

Eq.(4) can be non-dimensionalized, via the similarity variables

$$X = \frac{x}{H}, \quad Y = \frac{y}{H}, \quad \Psi(Y) = \frac{\hat{z}e\psi}{k_b \hat{T}}, \quad \rho^*(Y) = \frac{\rho_e}{n_0 \hat{z}e}, \tag{5}$$

in the following forms

$$\frac{d^2\Psi(Y)}{dY^2} = \kappa^2 \sinh(\Psi(Y)). \tag{6}$$

$$\frac{d^2\Psi(Y)}{dY^2} = -\frac{\kappa^2}{2}\rho^*(Y). \tag{7}$$

where $\kappa = H\,k$ in which $k^2 = 2n_0 \hat{z}^2 e^2/(\varepsilon_0 \varepsilon k_b \hat{T})$ is the Debye-Hückel parameter, and $1/k$ is normally regard as the EDL thickness.

The appropriate boundary conditions for Eqs.(6) and (7) are

$$\Psi(\pm 1) = \bar{\zeta} = \frac{\hat{z}e\zeta}{k_b \hat{T}}, \tag{8}$$

where ζ is the zeta potential measuring the electrical potential at the shear plane, i.e., the boundary between the compact layer and the diffuse layer [6].

If the electrical potential is small compared to the thermal energy of the ions, i.e., $(|\hat{z}e\psi| < |k_b\hat{T}|)$, using the Debye-Hückel linear approximation, Eq.(6) takes the form

$$\frac{d^2\Psi(Y)}{dY^2} = \kappa^2\Psi(Y), \tag{9}$$

which has the analytical solution

$$\Psi(Y) = \frac{\overline{\zeta}}{1+e^{2\kappa}}\left[e^{\kappa(1+Y)} + e^{\kappa(1-Y)}\right]. \tag{10}$$

3 Mathematical formulation for other fields

The nanofluid flow and heat transfer through a horizontal rectangular microchannel in the presence of the effects of EDL is investigated. The physical sketch is shown in Fig.1. Here x-axis is paralleled to the channel walls and y-axis is perpendicular to the walls. The origin of the coordinates is fixed at the centerline of the microchannel. H is the half distance between the upper and lower walls, L is the length of the microchannel, W is the width of the microchannel. To simplify the model without violating real physical circumstances, we assume that $W \gg H$, so that the problem can be formulated as a two-dimensional nonlinear microchannel flow problems in the presence of EDL effects.

The governing equations including the conservations of the total mass, the momentum,

the thermal energy and the nanoparticle volumetric fraction are expressed by

$$\nabla \cdot \mathbf{V} = 0, \tag{11}$$

$$\rho(\mathbf{V} \cdot \nabla)\mathbf{V} = -\nabla p + \mu \nabla^2 \mathbf{V} + \mathbf{F}, \tag{12}$$

$$(\mathbf{V} \cdot \nabla)T = \alpha \nabla^2 T + \tau \left[D_B \nabla T \cdot \nabla C + \left(\frac{D_T}{T_0} \right) \nabla T \cdot \nabla T \right] + \frac{\mu}{\rho c} \Phi, \tag{13}$$

$$(\mathbf{V} \cdot \nabla)C = D_B \nabla^2 C + \left(\frac{D_T}{T_0} \right) \nabla^2 T, \tag{14}$$

where $\mathbf{F}$ is the electrical body force. Φ is the viscous dissipation term, defined by

$$\Phi = 2 \left[\left(\frac{\partial u}{\partial x} \right)^2 + \left(\frac{\partial v}{\partial y} \right)^2 + \left(\frac{\partial w}{\partial z} \right)^2 \right] + \left(\frac{\partial v}{\partial x} + \frac{\partial u}{\partial y} \right)^2 + \left(\frac{\partial w}{\partial y} + \frac{\partial v}{\partial z} \right)^2 + \left(\frac{\partial u}{\partial z} + \frac{\partial w}{\partial x} \right)^2 - \frac{2}{3} \left(\frac{\partial u}{\partial x} + \frac{\partial v}{\partial y} + \frac{\partial w}{\partial z} \right)^2. \tag{15}$$

For parallel flow in channels, it is known that only one velocity component is not equal to zero, that means all fluid particles moving in the same direction. If, for example, only the velocity component u is nonzero, and thus v is everywhere zero, it follows immediately from the continuity equation that $\partial u/\partial x = 0$ and therefore u is independent of x. Similarly, the hydraulic pressure p is only dependent on the fluid motion, which indicates that it is only a function of x and therefore the pressure gradient dp/dx is constant. It is assumed that the temperature and the nanoparticle volumetric fraction on both walls increase or decrease linearly with x, namely, $T_w(x) = T_0 + A_1 x$ and $C_w(x) = C_0 + A_2 x$, where T_0 and C_0 are the reference temperature and the reference nanoparticle volumetric fraction at the channel entrance, respectively. Since the temperature T and the nanoparticle volumetric fraction C vary linearly with x [25, 26], we obtain $\dfrac{\partial^2 T}{\partial x^2} = \dfrac{\partial^2 C}{\partial x^2} = 0$.

Under those assumptions, the continuity equation is automatically satisfied, and other

governing equations are reduced to

$$\mu\frac{\partial^2 u}{\partial y^2} - \frac{\partial p}{\partial x} + E_x\rho_e = 0, \tag{16}$$

$$u\frac{\partial T}{\partial x} = \alpha\frac{\partial^2 T}{\partial y^2} + \tau D_B\left(\frac{\partial T}{\partial x}\frac{\partial C}{\partial x} + \frac{\partial T}{\partial y}\frac{\partial C}{\partial y}\right) + \frac{\tau D_T}{T_0}\left[\left(\frac{\partial T}{\partial x}\right)^2 + \left(\frac{\partial T}{\partial y}\right)^2\right] + \frac{\mu}{\rho c}\left(\frac{\partial u}{\partial y}\right)^2, \tag{17}$$

$$u\frac{\partial C}{\partial x} = D_B\frac{\partial^2 C}{\partial y^2} + \frac{D_T}{T_0}\frac{\partial^2 T}{\partial y^2}, \tag{18}$$

subject to the boundary conditions

$$u(\pm H) = 0, \quad T_w(\pm H) = T_0 + A_1\, x, \quad C_w(\pm H) = C_0 + A_2\, x. \tag{19}$$

It is a common practice in channel flow studies to assume the mass flow rate as a prescribed quantity. We thus obtain

$$U_m = \frac{1}{2H}\int_{-H}^{+H} u(y)dy = \frac{1}{H}\int_0^{+H} u(y)dy, \tag{20}$$

where U_m is the average fluid velocity in the channel section.

Define the dimensionless quantities

$$U(Y) = \frac{u}{U_m}, \quad \Theta(Y) = \frac{T - T_w}{A_1 H}, \quad \Phi(Y) = \frac{C - C_w}{A_2 H}. \tag{21}$$

Non-dimensionalize the momentum equation (16) by similarity transformations (5) and (21), we obtain

$$\frac{d^2U(Y)}{dY^2} + G_1 - 2G_2\bar{E}_s\Psi(Y) = 0, \tag{22}$$

subjected to the boundary conditions

$$U(\pm 1) = 0, \quad \int_0^1 U(Y)dY = 1, \tag{23}$$

where

$$G_1 = \frac{H^2}{\mu U_m}P_x, \quad G_2 = \frac{n_0\hat{z}e\zeta H^2}{\mu U_m L},$$

in which $P_x = -\dfrac{dp}{dx}$ is the pressure constant, $\bar{E}_s = E_s/\zeta$ is the stream potential, and $E_x = E_s/L$.

Substituting the non-dimensional variables (21) into Eqs.(17) and (18), we obtained the reduced energy equation and concentration of nanoparticles equation as

$$\Theta'' + Nb(1 + \Theta'\Phi') + Nt\left(1 + \Theta'^2\right) + PrEcU'^2 - RePrU = 0, \tag{24}$$

$$\Phi'' + \frac{Nt}{Nb}\Theta'' - RePrLeU = 0, \tag{25}$$

subject to following boundary conditions

$$\Theta(\pm 1) = 0, \quad \Phi(\pm 1) = 0, \tag{26}$$

where $Nb = \dfrac{\tau D_B A_2 H}{\alpha}$ is the Brownian motion parameter, $Nt = \dfrac{\tau D_T A_1 H}{\alpha T_0}$ is the thermophoresis parameter, $Pr = \dfrac{\nu}{\alpha}$ is the Prandtl Number, $Re = \dfrac{U_m H}{\nu}$ is the Reynolds Number, $Ec = \dfrac{U_m^2}{cA_1 H}$ is the Eckert number, $Le = \dfrac{\alpha}{D_B}$ is the Lewis number, respectively.

The physically important quantities of practical interests are the local skin friction, the local Nusselt number, the local Sherwood number. Since the flow is symmetric in the channel, we only need to consider them on the lower wall. In this case, they are defined by

$$C_{f2} = \frac{\tau_{w2}}{\rho_f U_m^2}, Nu_2 = \frac{x\, q_{wT2}}{k_f(T_w - T_0)}, \quad Sh_2 = \frac{x\, q_{wC2}}{D_B(C_w - C_0)}, \tag{27}$$

where

$$\tau_{w2} = \mu\left(\frac{\partial u}{\partial y}\right)_{y=-H}, \quad q_{wT2} = -k_f\left(\frac{\partial T}{\partial y}\right)_{y=-H}, \quad q_{wC2} = -D_B\left(\frac{\partial C}{\partial y}\right)_{y=-H}. \tag{28}$$

Substituting Eq.(21) into Eq.(27), we obtain

$$C_{f2} = \frac{1}{Re}U'(-1), \quad Nu_2 = -\Theta'(-1), \quad Sh_2 = -\Phi'(-1). \tag{29}$$

4 Explicit solution for the flow field

From Eq.(22) and its boundary conditions (23), the analytical solution for the reduced velocity field is obtained as

$$U(Y) = \frac{G_1}{2}(1 - Y^2) + \frac{2\bar{E}_s G_2 \bar{\zeta}}{\kappa^2}\left[\frac{\cosh(\kappa Y)}{\cosh(\kappa)} - 1\right]. \tag{30}$$

It is noted that the pressure constant G_1 and the dimensionless streaming potential $\bar{E}_s$ are not known yet, which will be determined as follow. Using the integral boundary conditions for $U(Y)$ denoted in Eq.(23), the relationship between G_1 and $\bar{E}_s$ are obtained:

$$\frac{G_1}{3} - \frac{2\bar{E}_s G_2 \bar{\zeta}}{\kappa^2} + \frac{2\bar{E}_s G_2 \bar{\zeta} \sinh(\kappa)}{\kappa^3 \cosh(\kappa)} = 1. \tag{31}$$

Physically, it is known that the electrical field is generated as an electrolyte is driven by a hydrostatic pressure through a microchannel with charged walls, which results in a streaming current, defined by

$$I_s = \int_{A_c} u \rho_e dA_c.$$

Using Eqs.(5), (7), and (21), we obtain its dimensionless form

$$I_s = -4U_m n_0 \hat{z} e W H \int_0^1 U(Y)\Psi(Y) dY. \tag{32}$$

On the other hand, the streaming potential produces a conduction current in the reverse direction, which is given by

$$I_c = \frac{\lambda_0 E_s A_c}{L}, \tag{33}$$

where λ_0 is the constant electrical conductivity of the fluid, A_c is the cross-sectional area of the channel. It can be transformed, using the relations $\bar{E}_s = E_s/\zeta$ and $A_c = 2H \times W$, into the following form

$$I_c = \lambda_0 \zeta \frac{2HW}{L} \bar{E}_s. \tag{34}$$

The electrokinetic potential E_x can be obtained by balancing the streaming current and the electrical conduction current at the steady state. In this situation, the net electrical current equates to zero, which indicates

$$I = I_s + I_c = 0. \tag{35}$$

Using Eqs.(34) and (32), $\bar{E}_s$ is obtained

$$\bar{E}_s = 2G_3 \int_0^1 U(Y)\Psi(Y)dY, \tag{36}$$

where $G_3 = \dfrac{LU_m n_0 \hat{z} e}{\lambda_0 \zeta}$ is a constant.

Substituting Eqs.(10) and (30) into Eq.(36), the other relationship between G_1 and $\bar{E}_s$ is obtained:

$$\bar{E}_s - \frac{2G_3\bar{\zeta}\left[G_1\kappa + \bar{E}_s G_2 \kappa\bar{\zeta}\mathrm{sech}^2(\kappa) - (G_1 + \bar{E}_s G_2\bar{\zeta})\tanh(\kappa)\right]}{\kappa^3} = 0. \tag{37}$$

Therefore, G_1 and $\bar{E}_s$ can be determined, via combining Eq.(31) and Eq.(37), as

$$G_1 = \frac{3\kappa^6 - 6\kappa^3 G_2 G_3 \bar{\zeta}^2[\kappa \mathrm{Sech}^2(\kappa) - \tanh(\kappa)]}{\kappa^6 - 2G_2 G_3 \bar{\zeta}^2[6\kappa^2 + \kappa^4 \mathrm{Sech}^2(\kappa) - \kappa\,(12+\kappa^2)\tanh(\kappa) + 6\tanh^2(\kappa)]},$$
$$\bar{E}_s = \frac{6G_3\kappa^3\bar{\zeta}[\kappa - \tanh(\kappa)]}{\kappa^6 - 2G_2 G_3 \bar{\zeta}^2[6\kappa^2 + \kappa^4 \mathrm{sech}^2(\kappa) - \kappa\,(12+\kappa^2)\tanh(\kappa) + 6\tanh^2(\kappa)]}.$$

Hence the explicit solution $U(Y)$ denoted in Eq.(30) is fully determined.

5 HAM solution and discussion

It is worth mentioning that the Eq.(22) contains two unknown constants G_1 and $\int_0^1 U(Y)\Psi(Y)dY$, which are difficult to be calculated directly by either numerical or analytical methods without special treatments. To overcome this limitation, we employ and extend the homotopy analysis method (HAM) [27] to obtain the accurate solutions of the nonlinear equations Eqs.(9), (22), (24) and (25), in which the exact values for G_1 and $\int_0^1 U(Y)\Psi(Y)dY$, are

calculated spontaneously and simultaneously as part of the solution procedure without any approximations.

We first define G_1 and $\int_0^1 U(Y)\Psi(Y)dY$ as

$$G_1 = \sigma = \sigma_0 + \sum_{j=1}^{\infty} \sigma_j, \quad \int_0^1 U\Psi dY = w = w_0 + \sum_{j=1}^{\infty} w_j, \tag{38}$$

then express the functions $\Psi(Y)$, $U(Y)$, $\Theta(Y)$ and $\Phi(Y)$ as

$$\begin{aligned} \Psi(Y) &= \psi_0(Y) + \sum_{j=1}^{\infty} \psi_j(Y), \quad U(Y) = u_0(Y) + \sum_{j=1}^{\infty} u_j(Y), \\ \Theta(Y) &= \theta_0(Y) + \sum_{j=1}^{\infty} \theta_j(Y), \quad \Phi(Y) = \phi_0(Y) + \sum_{j=1}^{\infty} \phi_j(Y). \end{aligned} \tag{39}$$

In the framework of the HAM, the kth order HAM deformation equations can be written as

$$\psi_m'' - \chi_m \psi_{m-1}'' = \hbar_\psi R_{\psi,m}, \tag{40}$$

$$u_m'' - \chi_m u_{m-1}'' = \hbar_u R_{u,m}, \tag{41}$$

$$\theta_m'' - \chi_m \theta_{m-1}'' = \hbar_\theta R_{\theta,m}, \tag{42}$$

$$\phi_m'' - \chi_m \phi_{m-1}'' = \hbar_\phi R_{\phi,m}. \tag{43}$$

subject to the boundary conditions

$$\psi_m(\pm 1) = 0, \quad u_m(\pm 1) = 0, \quad \int_0^1 u_m = 1, \quad \theta_m(\pm 1) = 0, \quad \phi_m(\pm 1) = 0, \tag{44}$$

where $\hbar_\psi$, $\hbar_u$, $\hbar_\theta$ and $\hbar_\phi$ are the HAM auxiliary parameters used for the convergence-control of the HAM analytical approximations. Also, $R_{\psi,m}$, $R_{u,m}$, $R_{\theta,m}$, $R_{\phi,m}$ and χ_m are defined,

respectively, by

$$R_{\psi,m} = \psi''_{m-1} - \kappa^2 \psi_{m-1} \tag{45}$$

$$R_{u,m} = u''_{m-1} + \sigma_{m-1} - 4G_2G_3 \sum_{j=0}^{m-1} w_j \psi_{m-1-j}, \tag{46}$$

$$\begin{aligned} R_{\theta,m} = \theta''_{m-1} + \sum_{j=0}^{m-1} \Big(Nb\, \theta'_j \phi'_{m-1-j} + Nt\, \theta'_j \theta'_{m-1-j} + PrEc\, u'_j u'_{m-1-j} \Big) \\ -RePr\, u_{m-1} + (Nt + Nb) * (1 - \chi_m) \end{aligned} \tag{47}$$

$$R_{\phi,m} = \phi''_{m-1} + \frac{Nt}{Nb} \theta''_{m-1} - RePrLe\, u_{m-1}, \tag{48}$$

where

$$\chi_m = \begin{cases} 0 & m \leq 1, \\ 1 & m > 1. \end{cases} \tag{49}$$

Here the expression (36) is used to obtain $R_{u,m}$.

The solutions of Eqs.(40)-(43) are in the forms of

$$\psi_m = \psi^* + \chi_m \psi_{m-1} + C_{1,m} + C_{2,m} Y, \tag{50}$$

$$u_m = u^* + \chi_m u_{m-1} + C_{3,m} + C_{4,m} Y, \tag{51}$$

$$\theta_m = \theta^* + \chi_m \theta_{m-1} + C_{5,m} + C_{6,m} Y, \tag{52}$$

$$\phi_m = \phi^* + \chi_m \phi_{m-1} + C_{7,m} + C_{8,m} Y, \tag{53}$$

where

$$\begin{aligned} \psi^* = \int\int \hbar_\psi R_{\psi,m} dY dY, \quad u^* = \int\int \hbar_u R_{u,m} dY dY, \\ \theta^* = \int\int \hbar_\theta R_{\theta,m} dY dY, \quad \phi^* = \int\int \hbar_\phi R_{\phi,m} dY dY. \end{aligned} \tag{54}$$

The integral constants $C_{i,m}$ $(i = 1, 2, 3, 4, 5, 6, 7, 8)$ are determined by the boundary conditions

$$C_{1,m} = -\frac{\psi^*(1) + \psi^*(-1)}{2}, \;\; C_{2,m} = -\frac{\psi^*(1) - \psi^*(-1)}{2}, \;\; C_{3,m} = -\frac{u^*(1) + u^*(-1)}{2},$$

$$C_{4,m} = -\frac{u^*(1) - u^*(-1)}{2}, \;\; C_{5,m} = -\frac{\theta^*(1) + \theta^*(-1)}{2}, \;\; C_{6,m} = -\frac{\theta^*(1) - \theta^*(-1)}{2}$$

$$C_{7,m} = -\frac{\phi^*(1) + \phi^*(-1)}{2}, \quad C_{8,m} = -\frac{\phi^*(1) - \phi^*(-1)}{2}.$$

The above HAM solution procedure can work accordingly after the initial approximations $\psi_0(Y)$, $u_0(Y)$, $\theta_0(Y)$ and $\phi_0(Y)$ are chosen properly based on the boundary conditions (44), such as

$$\psi_0(Y) = \bar{\zeta} Y^2, \quad u_0(Y) = 1 + \frac{3}{2}Y^2 - \frac{5}{2}Y^4,$$
$$\theta_0(Y) = 1 - Y^2, \quad \phi_0(Y) = 1 - Y^2. \tag{55}$$

During the HAM solution procedure, the unknown constant G_1 is determined in the following way. It is known that u_m contains the unknown term σ_{m-1}, which is determined using the mass flow rate equation(20). For instance, in the case of $\hbar_u = -1$, $G_2 = G_3 = 1$, $\bar{\zeta} = 1$, for the zero-th order approximation when $m = 1$, it is easily seen that u_1 contains the unknown term σ_0. By means of Eq.(20) we have

$$\int_0^1 u_1 dY = 0 \tag{56}$$

we can obtained the value of $\sigma_0 = \frac{1691}{525}$ from above equation. Also, the constant integration term $w_0 = \int_0^1 u_0(Y)\psi_0(Y)dY$ can be obtained by means of Eq.(55). In this way, the whole solution series in Eq.(38) for G_1 and the constant integration term can be determined successively from $m = 1, 2, 3, \cdots$.

To check the accuracies of the results, the error estimation function is defined as

$$E(m) = max\{E_\Psi(m), E_U(m), E_\Theta(m), E_\Phi(m)\}, \tag{57}$$

where

$$E_{\Psi}(m) = \int_{-1}^{1} (\Psi'' - \kappa^2 \Psi)^2 dY,$$
$$E_{U}(m) = \int_{-1}^{1} \left[U'' + G_1 - \left(4G_2 G_3 \int_0^1 U\Psi dY \right) \Psi \right]^2 dY,$$
$$E_{\Theta}(m) = \int_{-1}^{1} \left[\Theta'' + Nb(1 + \Theta'\Phi') + Nt\left(1 + \Theta'^2\right) + PrEcU'^2 - RePrU \right]^2 dY,$$
$$E_{\Phi}(m) = \int_{-1}^{1} \left(\Phi'' + \frac{Nt}{Nb}\Theta'' - RePrLeU \right)^2 dY.$$

Substituting mth order computational results into Eq.(57), the corresponding error can be obtained. In present work, the study mainly focuses on the effect of various physical quantities with the κ value ranging from 0 to 20. The rest of the dimensionless parameters are given the fixed values. For instance, in the case of $G_2 = G_3 = 1$, $Ec = Le = Re = 1, \bar{\zeta} = 1, Pr = 5, Nt = 1/10, Nb = 2/10$, we obtain the maximum error $E(m)$ for various values of κ, as listed in Table 2. Note that the Homotopy-Padé technique [27] is employed to improve the convergence of the HAM approximations.

It is noted that Mala *et al.* [8] gave an analytical solution for $\Psi(y)$, by imposing an additional boundary condition $\Psi(0) = 0$, as

$$\Psi(Y) = \frac{\bar{\zeta}}{\sinh(\kappa)} |\sinh(\kappa Y)|. \tag{58}$$

The solution exists singularity at $Y = 0$ and is physically unrealistic, as shown in Fig.2. It can be seen in the figure that the present analytical solution denoted in Eq.(10) are structurally different from the result given by Mala *et al.* [8,9]. They are smooth for all κ. As κ becomes sufficiently large, $\Psi(Y)$ diminishes to zero in the middle of the channel. This is due to the important assumptions of Zeta potential [6] in the application of micro-channels (i) the surface is flat and (ii) the double layer is able to develop fully so that the potential in the middle of the channels is zero. It is also noticed that the HAM solutions agree with the analytical ones (10) in the whole region $-1 \leq Y \leq 1$ for all considered κ.

The solution of Mala *et al.* (58) for the electrostatic potential exists singularity at $Y = 0$, causes the velocity profiles discontinuous at the same place, the less is κ, the clearer is the discontinuity, as shown in Fig.3. Obviously, the solution is against the natural laws and physically impossible, while the present analytical solution (30) is consecutive and smooth in the whole region. Particularly when κ is sufficiently large, Mala's result seems to match the present solution, but in this case, the distance between two plates is too large to describe the microchannel flow with interfacial electrokinetic effects. In Fig.3, it is seen that the HAM approximation agrees well with the analytical solution (30). This further confirms the validity and accuracy of the present HAM solutions.

The influence of κ on the pressure constant G_1 is presented in Fig.4. It is shown that G_1 decreases monotonously as κ evolves. It is noted that as the value of κ decreases, the microchannel is narrower, thus the electric double layer effect is stronger. The electric double layer leads to back flow near the channel wall which could induce a stronger flow resistance in the microchannel, thus further lead the pressure constant increases. On the contrary, as κ increases, the distance between the microchannel wall becomes larger, the electric double layer effect is weak, the fluid flow is not affected by electric double layer, so the pressure tends to be a constant. Viewed from another perspective, if we keep the distance between the two plates remains unchanged, then κ is inversely proportional to the thickness of electrical double layer. The larger is κ, the thinner is the thickness of electric double layer. As κ is considerably large, the thickness of electric double layer approaches to zero. In this situation, the electrical double layer effect on the fluid motion can also be ignored.

The streaming potential E_s is an important factor to affect the flow patterns in the microchannel. As shown in Fig.5, $\bar{E}_s$ decreases very quickly as κ evolves. It is sufficient to

show that $\bar{E}_s$ approaches to zero with κ being considerably large. In fact, the reason of this phenomenon can be explained from the point of the electrical double layer. The rising value of κ may be due to the increasing bulk concentration of ions. Accordingly, the counter-ions concentration in the liquid increases, which leads to the diffuse layer compressed. With more counter-ions being extruded into the shear plane, the zeta potential is thus decreased leading to a decreased streaming potential. If the bulk concentration is sufficiently large, namely the κ is large enough, the zeta potential will tend to zero, therefore the streaming potential also tend to zero.

In macroscopical flows, the effect of viscous dissipation on the fluid flow is usually small, therefore it could be ignored. But in microscopic ones, the viscous dissipation function can be very strong, and in turn its influence on the distribution of the flow temperature can be significant. As a result, it leads to the flow obviously changed in the microchannel. As seen in Fig.6, $\Theta(Y)$ increases rapidly with Ec increasing. It is also shown in Fig.7 that Ec has a significant effect on the nanoparticle concentration distribution $\Phi(Y)$. Its increase causes the rapid reduction of the relative nanoparticle concentration $\Phi(Y)$.

It is noted that the physical quantities such as the local skin friction, the local Nusselt number and the local Sherwood number are of importance in practical applications. It is therefore necessary to further examine discuss their variational trends with Re and κ on the lower wall in detail.

Many studies on microchannel flow, especially contains the effect of electric double layer, but less research with focus on Reynolds number. Thus, some results about the Reynolds number are presented in order to provide theoretical basis for test. From Table 3, it is found that the Reynolds number Re have great influence on both the local Nusselt number Nu_2 and the local Sherwood number Sh_2. The absolute value of Nu_2 decreases with the

increase of Re. However, the value of Sh_2 enhances with Re evolving. It is also noted that Sh_2 increases faster than Nu_2 indicating that the effect of Re on Sh_2 is greater than that of Nu_2. As shown in Fig.8, it is seen that C_{f2} decreases rapidly as κ increases when κ is small. It is worth mentioning that C_{f2} reaches a minimum near $\kappa = 1.5$. Once going over this minimum value, C_{f2} increases as κ evolves and approaches to 3 as κ keeps continuously increasing. It is observed that the large κ corresponds to the thin electric double layer thickness. Conversely, the small κ indicates the thick electric double layer thickness. It is illustrated in Fig.9 that the variation of local Nusselt number Nu_2 with κ exhibits the totally reverse trend relative to that of C_{f2}. The local Nusselt number Nu_2 rapidly increases to its maximum value, then gradually reduces as κ continuously increases. When κ becomes sufficiently large, the local Nusselt number Nu_2 closes to a certain constant. As shown in Fig.10, the influences of κ on the local Sherwood number Sh_2 are presented. It has the similar trend as the variation of C_{f2} with κ. Namely, Sh_2 decreases as κ increases for small κ. After reaching the minimum value, Sh_2 increases as κ evolves.

6 Conclusion

The nanofluid flow through a microchannel with the effects of the EDL are investigated. By eliminating the unphysical assumption leading to the discontinuities of flow field and replacing the inappropriate pressure constant assumption, the microchannel problem is re-formulated, which is consistent with commonly-accepted models in channels. The major findings contained in this paper are as follows:

1. The analytical solutions for both the electrostatic potential and the velocity field are given, which are consecutive and smooth in the whole region. These results are obviously better than those given by Mala *et al.* [8].

2. κ is a key factor to measure the EDL effects. It is noted that when $\kappa \geq 20$, its effects become negatively small. In this situation, the electrical double layer effect on the fluid motion and heat transfer can be ignored, thus the corresponding physical quantities tend to be constant, i.e. the streaming potential $\bar{E}_s$ approaches to zero. The pressure constant G_1, the local skin friction, the local Nusselt number and the local Sherwood number approach to fixed values, respectively.

3. The effect of viscous dissipation influence on the distribution of the fluid temperature and the nanoparticle concentration is significant. The reason is that the shear strength and frictional resistance are greatly increased in the microchannel, it leads to the viscous dissipation function is very strong.

References

[1] M. R. Safaei, M. Gooarzi, O.A. Akbari, M.S. Shadloo, M. Dahari, Performance evaluation of nanofluids in an inclined ribbed microchannel for electronic cooling applications. *Electronics Cooling*, (2016), DOI: 10.5772/62898.

[2] A. A. A. Arani, O. A. Akbari, M. R. Safaei, A. Marzban, A.A.A.A. Alrashed , Heat transfer improvement of water/single-wall carbon nanotubes (SWCNT) nanofluid in a novel design of a truncated double-layered microchannel heat sink. *International Journal of Heat and Mass Transfer*, 113, (2017) 780-795.

[3] A. B. Duncan, G. P. Peterson, Review of microscale heat transfer. *Applied Mechanics Reviews*, 47(9), (1994) 397-428.

[4] X. F. Peng, G. P. Peterson, B. X. Wang, Heat transfer characteristics of water flowing through microchannels. *Experimental Heat Transfer*, 7(4), (2012) 265-283.

[5] B. X. Wang, X. F. Peng , Experimental investigation on liquid forced-convection heat transfer through microchannels. *International Journal of Heat and Mass Transfer* , 37,(1994) 73-82.

[6] R.J. Hunter, Zeta Potential in Colloid Science, Principles and Applications. *Academic Press* , New York, 1981.

[7] C. Yang, D. Li , Analysis of electrokinetic effects on the liquid flow in rectangular microchannels. *Colloids and Surfaces A: Physicochemical and Engineering Aspects*, 143(2),(1998) 339-353.

[8] G. M. Mala, D. Li, J. D. Dale, Heat transfer and fluid flow in microchannels. *International Journal of Heat and Mass Transfer*, 40(13),(1997) 3079-3088.

[9] G. M. Mala, D. Li, C. Werner, H. J. Jacobasch, Y. B. Ning, Flow characteristics of water through a microchannel between two parallel plates with electrokinetic effects. *International Journal of Heat and Fluid Flow*, 18(5),(1997) 489-496.

[10] L. Ren, W. Qu, D. Li,Interfacial electrokinetic effects on liquid flow in microchannels. *International Journal of Heat and Mass Transfer*, 44(16),(2001) 3125-3134.

[11] Y. P. Zhang, T. W. Xu, Z. H. Liu, Streaming potential across a porous charged membrane in organic-aqueous solutions. *Desalination* , 212(1-3), (2007) 183-190.

[12] M. R. Safaei, A. H. Jahanbin, A. Kianifar, S. Gharehkhani, A.S. Kherbeet, Mathematical modeling for nanofluids simulation: a review of the latest works. *Modeling and Simulation in Engineering Sciences*, (2016), DOI: 10.5772/64154.

[13] A. Karimipour, A. H. Nezhad, A. D'Orazio, M. H. Esfe, M. R. Safaei , Simulation of copper-water nanofluid in a microchannel in slip flow regime using the lattice Boltzmann method. *European Journal of Mechanics - B/Fluids*, 49(49), (2015) 89-99.

[14] Z. Nikkhah, A. Karimipour, M. R. Safaei, P. Forghani-Tehrani, M. Goodarzi , Forced convective heat transfer of water/functionalized multi-walled carbon nanotube nanofluids in a microchannel with oscillating heat flux and slip boundary condition. *International Communications in Heat and Mass Transfer*, 68, (2015)69-77.

[15] D. Wen, Y. Ding, Experimental investigation into convective heat transfer of nanofluids at the entrance region under laminar flow conditions. *International Journal of Heat and Mass Transfer*, 47(24),(2004) 5181-5188.

[16] W. Williams, J. Buongiorno, L. W. Hu, Experimental investigation of turbulent convective heat transfer and pressure loss of alumina/water and zirconia/water nanoparticle colloids (nanofluids) in horizontal tubes. *Journal of Heat Transfer*, 130(4), (2008) 042412.

[17] M. R. Safaei, M. S. Shadloo, M. S. Goodarzi, A. Hadjadj, H. R. Goshayeshi , A survey on experimental and numerical studies of convection heat transfer of nanofluids inside closed conduits. *Advances in Mechanical Engineering*,8(10),(2016).

[18] Y. Xuan, Q. Li, Investigation on convective heat transfer and flow features of nanofluids. *Journal of Heat transfer*, 125(1),(2003) 151-155.

[19] Y. Yang, Z. G. Zhang, E. A. Grulke, W. B. Anderson, G. Wu, Heat transfer properties of nanoparticle-in-fluid dispersions (nanofluids) in laminar flow. *International Journal of Heat and Mass Transfer*, 48(6),(2005) 1107-1116.

[20] S. U. S. Choi, Enhancing thermal conductivity of fluids with nanoparticles, in: Proceedings of the 1995 ASME International Mechanical Engineering Congress and Exposition FED 231/ MD66, ASME, San Francisco, CA, USA, (1995) 99-106.

[21] Y. Xuan, W. Roetzel, Conceptions for heat transfer correlation of nanofluids. *International Journal of Heat and Mass Transfer*, 43(19),(2000) 3701-3707.

[22] J. Buongiorno, Convective transport in nanofluids.*Journal of Heat Transfer ASME*, 128(3), 2006 240-250.

[23] O. A. Bég, M. F. M. Basir, M. J. Uddin, A. I. M. Ismail, Numerical study of slip effects on unsteady asymmetric bioconvective nanofluid flow in a porous microchannel with an expanding/contracting upper wall using buongiornos model. *Journal of Mechanics in Medicine and Biology*, (2016)1750059.

[24] S. Tardu, The electric double layer effect on the microchannel flow stability. Microscale Thermophysical Engineering, 8(4),(2004) 383-401.

[25] A. S. Lavine, Analysis of fully developed opposing mixed convection between inclined parallel plates. *Wärme - und Stoffübertragung*, 23(4),(1988) 249-257.

[26] X. C. You, H. Xu, I. Pop, Analysis of fully developed opposing mixed convection flow in an inclined channel filled by a nanofluid, *Journal of Heat Transfer ASME*, 136,(2014) 124502-1-124502-5,

[27] S. J. Liao Homotopy analysis method in nonlinear differential equations. Higher Education Press; Springer, 2012.

Table 2: The maximum error $E(m)$

order	$\kappa = 1$	$\kappa = 3$	$\kappa = 5$	$\kappa = 20$
10	1711.196	13738.398	4686.691	70.382
20	8.002	0.793	0.125	0.798
30	1.87×10^{-7}	0.166	2.80×10^{-4}	6.50×10^{-4}
40	5.37×10^{-15}	1.49×10^{-4}	1.42×10^{-8}	2.82×10^{-5}
50	1.32×10^{-23}	7.17×10^{-7}	1.24×10^{-8}	1.097×10^{-5}
60	-	-	-	1.46×10^{-6}

Table 3: The results of Nu_2 and Sh_2 with variation of Re and κ in the case of $Le = Ec = 1$, $Nb = 1/5$, $Nt = 1/10$, $Pr = 5$, $G_2 = G_3 = 1$ and $\bar{\zeta} = 1$.

Re	$\kappa = 1$		$\kappa = 3$		$\kappa = 20$	
	Nu_2	Sh_2	Nu_2	Sh_2	Nu_2	Sh_2
1	-9.090	9.545	-9.119	9.559	-9.180	9.590
10	-2.088	51.044	-2.137	51.069	-2.247	51.123
20	-1.216	100.608	-1.249	100.625	-1.328	100.664
30	-0.843	150.421	-0.867	150.433	-0.927	150.464
40	-0.643	200.326	-0.662	200.331	-0.711	200.356
50	-0.520	250.291	-0.536	250.269	-0.576	250.291

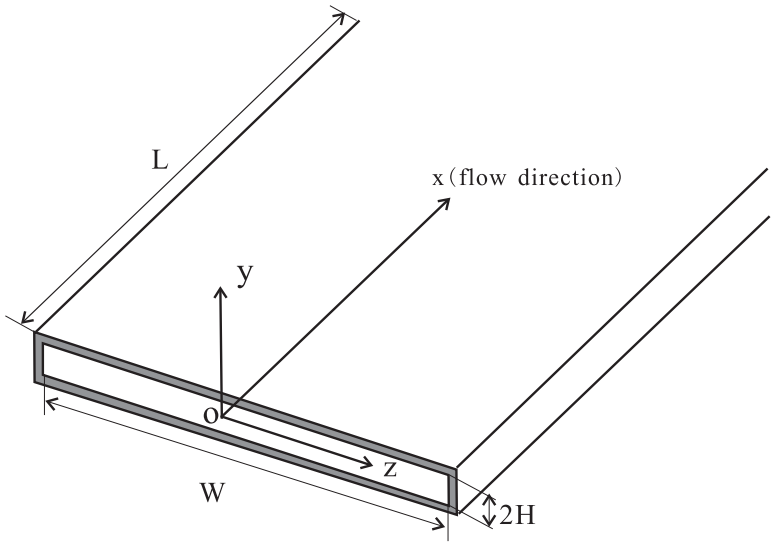

(a) 3-D sketch

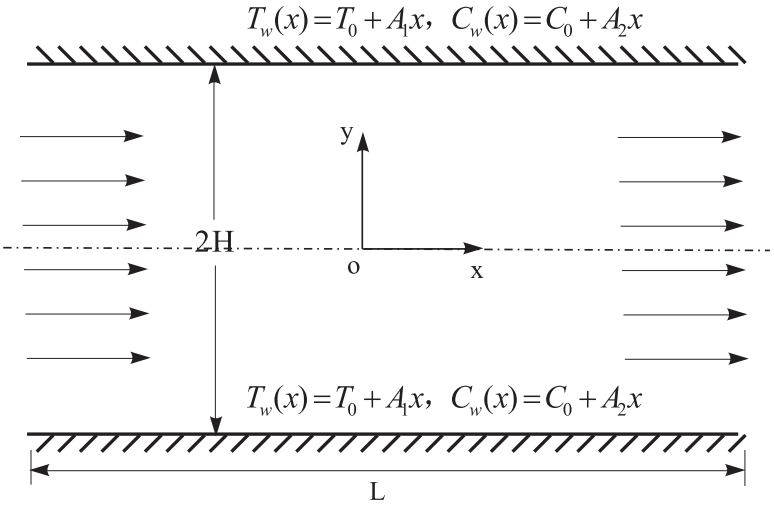

(b) 2-D sketch

Figure 1: Physical model and coordinate system

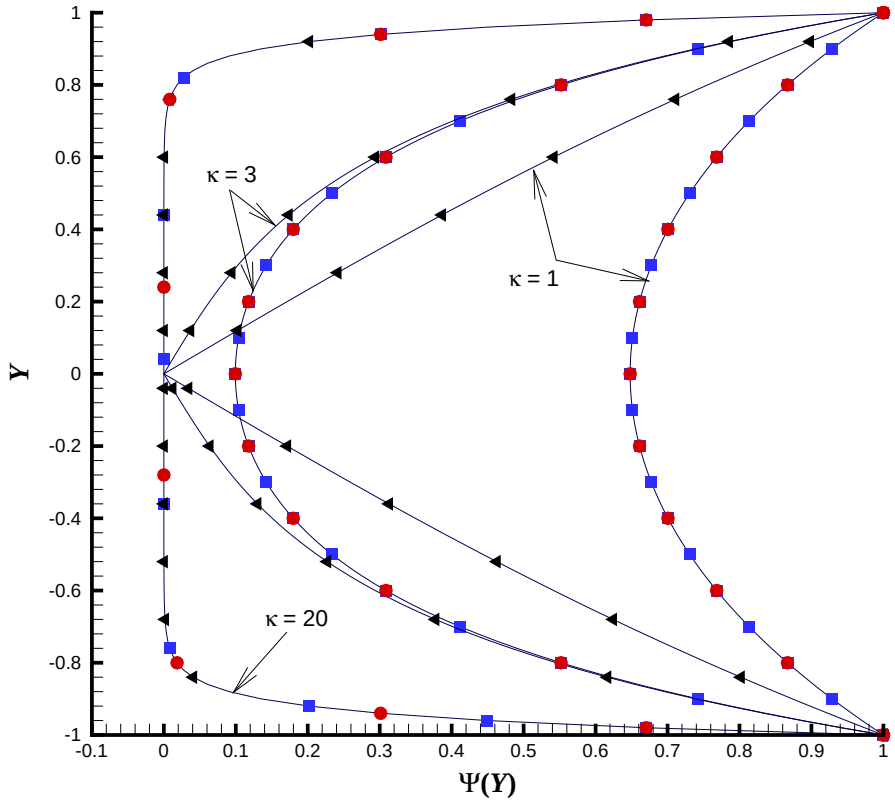

Figure 2: The electrical potential $\Psi(Y)$ for various values of κ with $\bar{\zeta} = 1$. Line with circles: analytical solutions given by Eq.(10); line with squares: HAM solutions; line with gradients: results of Mala *et al.* [8].

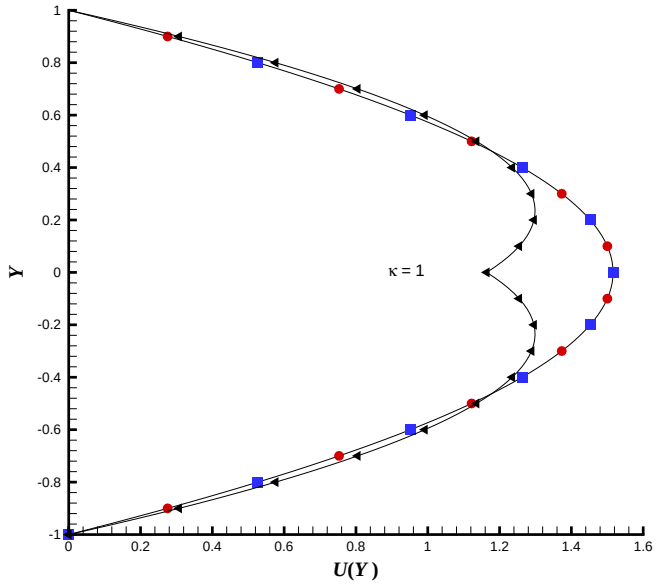

(a) $\kappa = 1$

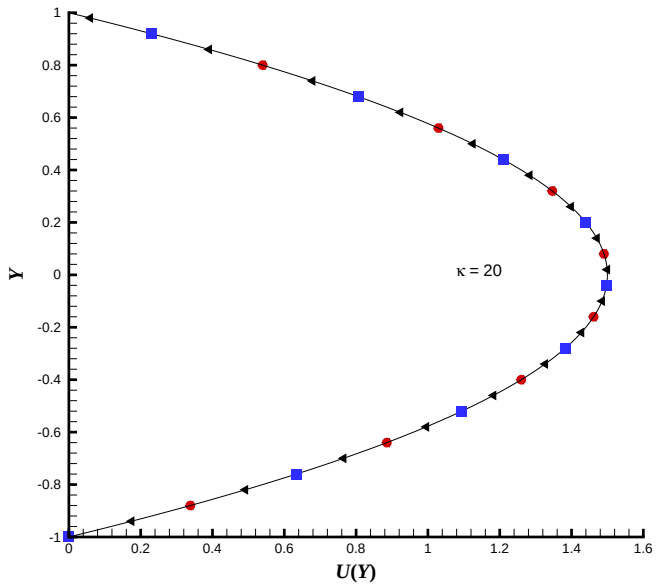

(b) $\kappa = 20$

Figure 3: The velocity $U(Y)$ for various values of κ with $G_2 = G_3 = 1$ and $\bar{\zeta} = 1$. Line with circles: analytical solutions given by Eq.(10); line with squares: HAM solutions; line with gradients: results of Mala *et al.* [8].

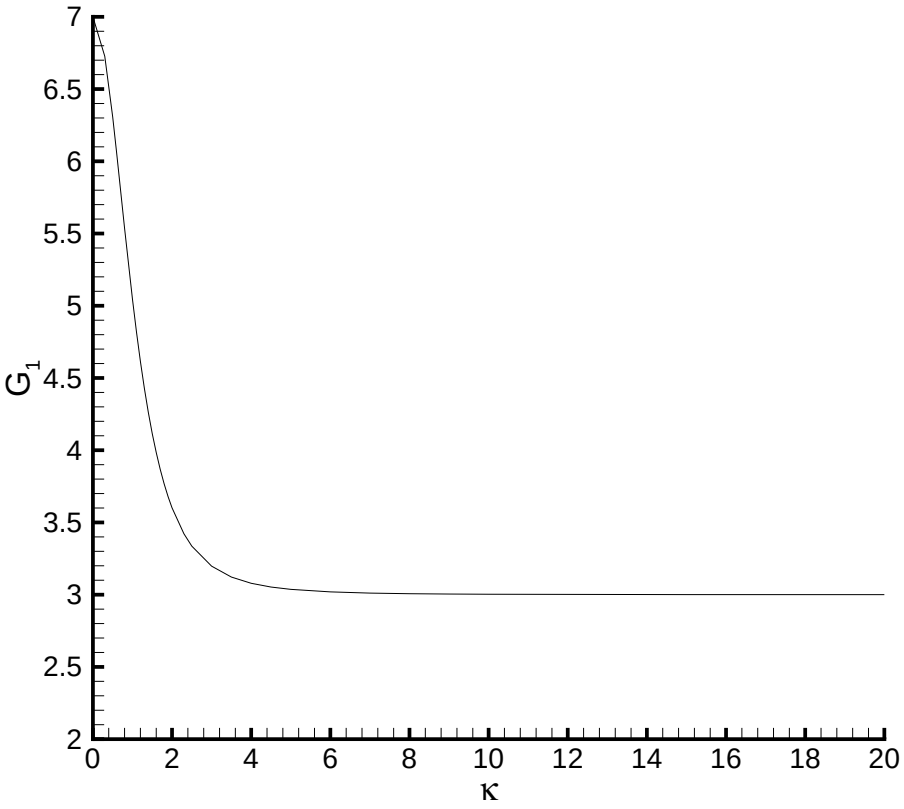

Figure 4: Variation of the pressure constant G_1 with κ in the case of $Ec = Le = Re = 1$, $Nb = 1/5$, $Nt = 1/10$, $Pr = 5$, $G_2 = G_3 = 1$ and $\bar{\zeta} = 1$.

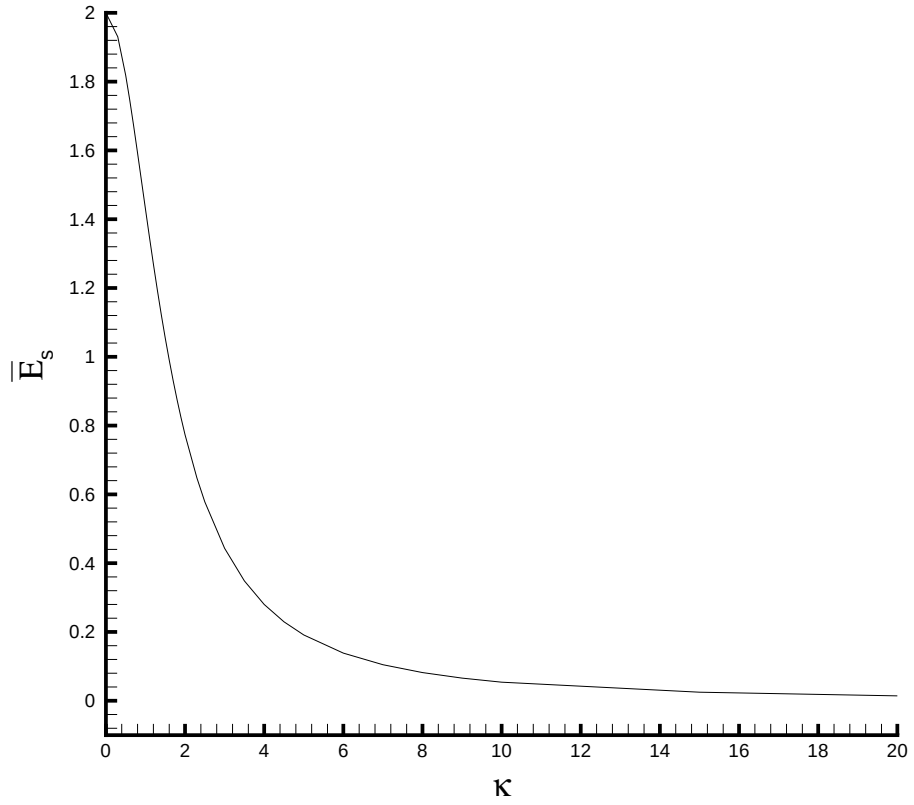

Figure 5: Variation of the streaming potential $\bar{E}_s$ with κ in the case of $Ec = Le = Re = 1$, $Nb = 1/5$, $Nt = 1/10$, $Pr = 5$, $G_2 = G_3 = 1$ and $\bar{\zeta} = 1$.

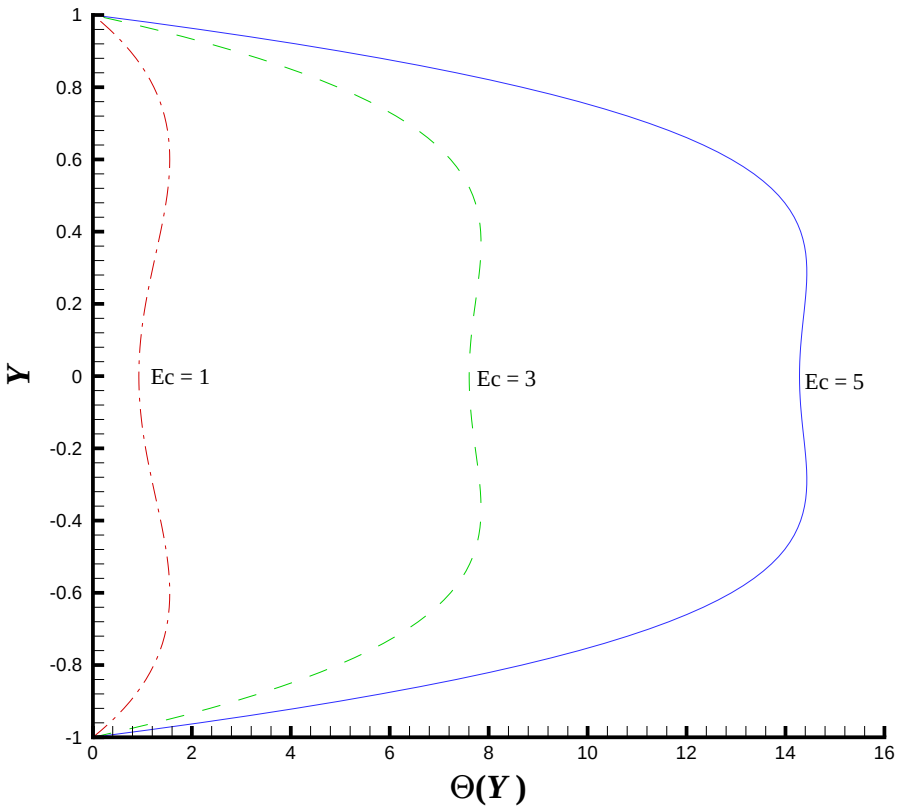

Figure 6: Variation of $\Theta(Y)$ with Ec in the case of $\kappa = 1$, $Le = Re = 1$, $Nb = 1/5$, $Nt = 1/10$, $Pr = 5$, $G_2 = G_3 = 1$ and $\bar{\zeta} = 1$.

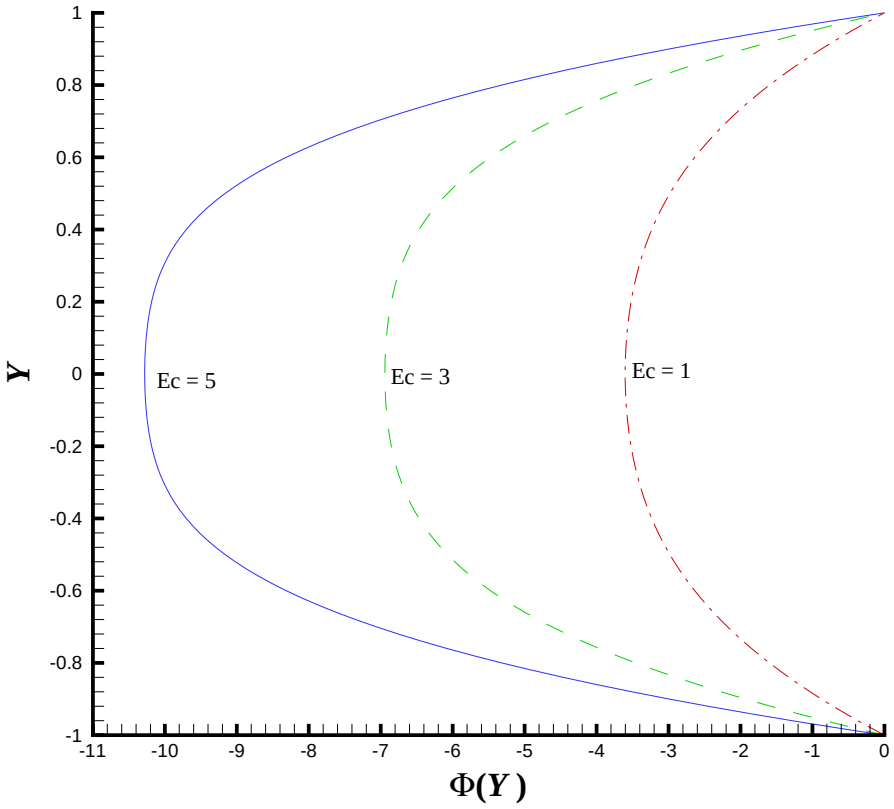

Figure 7: Variation of $\Phi(Y)$ with Ec in the case of $\kappa = 1$, $Le = Re = 1$, $Nb = 1/5$, $Nt = 1/10$, $Pr = 5$, $G_2 = G_3 = 1$ and $\bar{\zeta} = 1$.

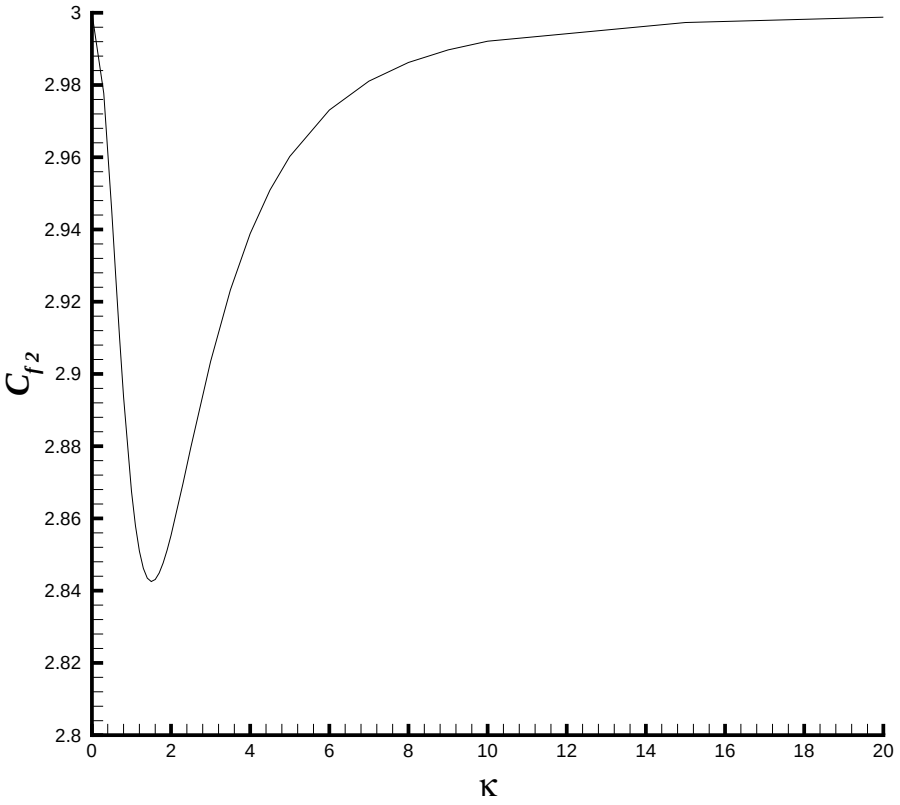

Figure 8: Variation of C_{f2} with κ in the case of $Ec = Le = Re = 1$, $Nb = 1/5$, $Nt = 1/10$, $Pr = 5$, $G_2 = G_3 = 1$ and $\bar{\zeta} = 1$.

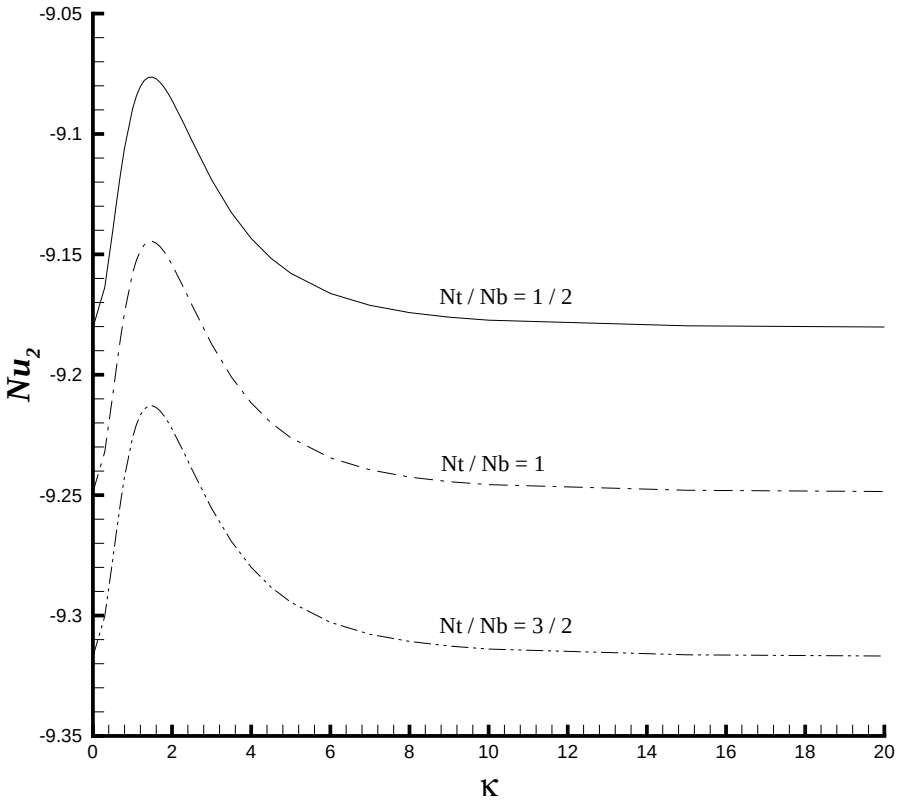

Figure 9: Variation of Nu_2 with κ in the case of $Ec = Le = Re = 1$, $Pr = 5$, $G_2 = G_3 = 1$ and $\bar{\zeta} = 1$.

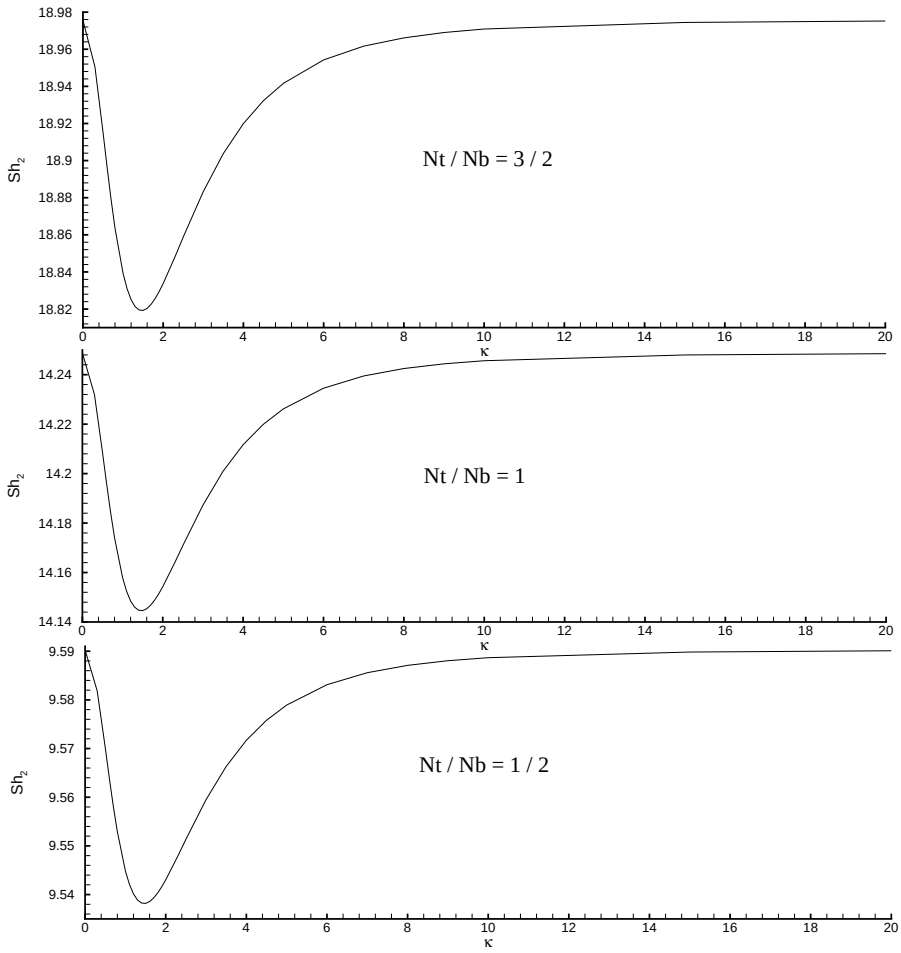

Figure 10: Variation of Sh_2 with κ in the case of $Ec = Le = Re = 1$, $Pr = 5$, $G_2 = G_3 = 1$ and $\bar{\zeta} = 1$.